Thesis for the degree of Licentiate of Engineering

On the Function of Ceria Supported Rhodium Catalysts for Methanation of Carbon Dioxide

Felix Hemmingsson

Department of Chemistry and Chemical Engineering

Chalmers University of Technology

Gothenburg, Sweden 2020

On the Function of Ceria Supported Rhodium Catalysts for Methanation of Carbon Dioxide

Felix Hemmingsson

Licentiatuppsatser vid Institutionen för kemi och kemiteknik
Chalmers tekniska högskola
Nr 2020:09

Department of Chemistry and Chemical Engineering
Chalmers University of Technology
SE-412 96 Gothenburg
Telephone +46 31 772 1000

Typeset in LaTeX using the kaobook class
Printed by Chalmers Reproservice
Gothenburg, Sweden 2020

On the Function of Ceria Supported Rhodium Catalysts for Methanation of Carbon Dioxide

Felix Hemmingsson
Department of Chemistry and Chemical Engineering
Chalmers University of Technology

Abstract

Technologies for energy harvesting of sustainable sources such as solar and wind lack an inherent energy buffer. As such, storing excess energy in chemical bonds, for example that of hydrogen (H_2), is a desirable complementary concept. While hydrogen gas is easily cycled and applied in electrical systems, it brings high costs for long term storage and transportation. The technical solutions introduce complications in terms of limited equipment lifetime and when applied in combustion systems also safety concerns. An alternative for these applications is to further convert the hydrogen into hydrocarbons such as alkanes and alcohols. Through CO_2 hydrogenation, methane can be produced and used in current infrastructure solutions due to it being the major component also in natural gas. While typically produced using nickel based catalysts, other metals such as ruthenium and rhodium have shown promise, of which Rh/CeO_2 is one such catalyst. While kinetic studies exist of said catalyst, the reaction mechanism is unknown, which hampers further development.

This work aims towards clarifying the catalyst structure-function relationship as well as the important surface reactions. The ambition is to facilitate the start of fundamental research approach, which can later be developed to achieve a more complete understanding, allowing for tuning the important properties of said catalyst.

In this work, Rh/CeO_2 catalysts were prepared by incipient wetness impregnation and studied *in situ* during CO_2 hydrogenation in regards to its structural behaviour, by the use of high-energy X-ray diffraction and ambient pressure X-ray photoelectron spectroscopy, as well as the surface reactions using diffuse reflectance infrared spectroscopy. As signals from processes and adsorbates that truly participate in the reaction may be hidden by spectator signals, these studies were performed transiently as to enhance the response of active species while decreasing that of spectators.

It was revealed that CeO_2 is active during reaction conditions, possibly partaking in a cycle of formation and healing of oxygen vacancies during the reaction cycle as evidenced by the cycling of Ce^{4+} and Ce^{3+}. Furthermore, while predominantly reduced, a RhO_x phase was observed, showing the strong metal support interaction of Rh and CeO_2. Regarding surface reactions, several carbonyl species (b-CO, h-CO, m-CO) were shown to be active on the catalyst, as well as some carbonates (b-CO_3, p-CO_3) and formate (b-HCOO) species.

While the complete pathway need more experimental data to be determined, the activity of the carbonyl species suggests that the reaction follows a carbon monoxide based pathway such as the carbide pathway.

Keywords: Sabatier reaction; CO_2 reduction; Catalytic methanation; Hydrogenation; *In situ* spectroscopy; HE-XRD; AP-XPS; DRIFTS

List of Publications

This thesis is based on the following appended papers:

I. Structure-function relationship for CO_2 methanation over ceria supported Rh and Ni catalysts at atmospheric pressure conditions

N. M. Martin, F. Hemmingsson, A. Schaefer, M. Ek, L. R. Merte, U. Hejral, J. Gustafson, M. Skoglundh, A.-C. Dippel, O. Gutowski, M. Bauer, and P.-A. Carlsson

Catalysis Science & Technology, 9 **(2019)**, *1644-1653*

II. CO_2 Methanation over Rh/CeO_2 Studied with Infrared Modulation Excitation Spectroscopy and Phase Sensitive Detection

F. Hemmingsson, A. Schaefer, M. Skoglundh and P.-A Carlsson

Submitted manuscript **(2020)**

My Contributions to the Publications

Paper I

I set-up and co-performed the HE-XRD experiments and co-authored the paper.

Paper II

I designed and performed all experiments and analyses, excluding XRF, and authored the manuscript.

Publications not included in the thesis:

Structure–function relationship during CO_2 methanation over Rh/Al_2O_3 and Rh/SiO_2 catalysts under atmospheric pressure conditions

N. M. Martin, F. Hemmingsson, X. Wang, L. R. Merte, U. Hejral, J. Gustafson, M. Skoglundh, D. M. Meira, A.-C. Dippel, O. Gutowski, M. Bauer and P.-A. Carlsson

Catalysis Science & Technology, 8 **(2018)**, *2686-2696*

Methane Adsorption and Methanol Desorption of Copper Modified Boron Silicate

X. Wang, A. Shishkin, F. Hemmingsson, M. Skoglundh, F. J. Martinez-Casado, L. Bock, A. Idström, L. Nordstierna, H. Härelind and P.-A. Carlsson

*RSC Advances, 8 (***2018***), 3639-36374*

Contents

Contents i

1 Introduction 1
1.1 Catalysis for energy applications . . . 2
1.2 Motivation of this work . . . 3

2 Background 5
2.1 The Sabatier reaction . . . 5
Proposed reaction mechanisms . . . 6
2.2 The importance of transient *in situ* studies to reveal reaction mechanisms . . . 6
2.3 Objectives . . . 7

3 Methodology 9
3.1 Catalyst preparation . . . 9
3.2 X-ray diffraction . . . 10
3.3 X-ray photoelectron spectroscopy . . . 11
3.4 Infrared spectroscopy . . . 11
Diffuse reflectance . . . 12
Molecular vibrations and selection rules . . . 13
3.5 Modulation excitation spectroscopy . . . 13
Phase-sensitive detection . . . 14

4 Results and discussion 17
4.1 Physico-chemical behaviour of the catalyst . . . 17
Observing the crystal structural dynamics . . . 17
Changes in the surface oxidation state . . . 18
4.2 Exploring the surface reactions . . . 18
Active and inactive, adsorbates at steady-state . . . 19
Active species – to separate the wheat from the chaff . . . 20
4.3 Reaction mechanisms – formulating an idea . . . 24

5 Conclusions and future work 27
5.1 Remaining questions . . . 27

Bibliography 31

Notation 35

List of Figures

1.1 Schematic energy diagram for a catalysed reaction 2

3.1 Illustration showing the effect of thermal drying during impregnation 9

3.2 Schematic representation of Bragg's law 10
3.3 Schematic diagram for the process of XPS 11
3.4 Schematic representation of transmission and reflectance 11
3.5 Difference between specular and diffusive reflection. 12
3.6 Schematic illustration of the DRIFTS cell 12
3.7 A conceptual sketch of a MES experiment 14
3.8 Simulated ME experiment with sinus modulation 15
3.9 Phase resolved data of simulated MES experiment 15
3.10 The sinusoidal composition of a square wave 16
4.1 TEM image of the Rh/CeO_2 catalyst 17

4.2 X-ray diffractogram of the *in situ* study of Rh/CeO_2 during CO_2 methanation . . 18
4.3 XPS spectra of the reduced and oxidised Rh/CeO_2 19
4.4 AP-XPS spectra of Rh/CeO_2 during CO_2 methanation 19
4.5 IR spectra during steady-state CO_2 adsorption and methanation on Rh/CeO_2 . 20
4.6 Contour plot of the IR-MES data in the time domain 21
4.7 Result of the IR-MES-PSD study 22
4.8 The phase resolved spectra for the OH and CH vibrations 24

List of Tables

3.1 The six normal modes of vibration, applied to the CO_2 molecule. 13

4.1 Infrared peak assignments for the transient experiments. 23

1 Introduction

The search for sustainable energy sources and systems has amassed a significant interest among societal actors, engineers and researchers. While the focus often, and perhaps foremost, has been on the availability of energy sources, an important shift towards questions regarding energy storage and fuels that are not sourced from fossil reserves has been witnessed during the latest decades [1, 2]. Though energy harvesting by wind and solar power shows great promise as "green" energy solutions [3], their dependence on external factors, e.g., weather, season and grid load, make them lack the necessary on-demand energy supply capability [4]. This currently limits their possibility of constituting a larger portion of countries' energy system if not an energy buffer can be introduced. One such buffer could be the formation of gaseous hydrogen (H_2) by for instance water splitting (eq. (1.1)). Thereby the obtained energy is chemically stored in the hydrogen bond. This concept could be set up as a closed system by recycling the constituent molecules and is thus characterised by a zero net consumption/production of H_2O/H_2 [5].

$$2\,H_2O \rightleftharpoons 2\,H_2 + O_2 \tag{1.1}$$

Indeed, the concept of using H_2 as a basal energy vector has by itself gained much attention and the concept has been coined the *hydrogen economy*[6]. Even if H_2 is easily cycled and suitable applied in electrical systems, by the use of fuel cells [7], there are still a number of inherent problems associated with the broader use of H_2. For combustion systems, for example, a small H_2 concentration in the gas stream is tolerable[1] but higher concentrations poses safety risks in terms of corrosion, i.e., hydrogen embrittlement, with consequential risk of leakage [9–11]. Furthermore, due to it being a gas at normal conditions, which is relevant for the majority applications, H_2 lacks the appropriate energy density and has a high storage cost in comparison to other fuels [12]. In order to circumvent these problems, it is possible to convert H_2 into alkanes and alcohols by hydrogenation of carbon oxides, i.e., carbon monoxide (CO) and carbon dioxide (CO_2) [2]. In contrast to H_2, long-chained alkanes and alcohols are liquids at normal conditions and can often be applied directly[2] in existing systems such as combustion engines. However, while obtaining high energy densities and low storage costs, the processes for the production of these fuels incur an energy loss[3] and require expensive high-

1: Furthermore, for certain applications an addition of hydrogen could prove beneficial, such as the case of utilisation of hydromethane (natural gas and hydrogen mixtures) [8].

2: Or with minor adjustments [13]. Furthermore, as these are base chemicals they are also of interest for applications other than fuel.

3: As an example, $\Delta H_f^\circ(CH_3OH(g)) = -201.17\,\mathrm{kJ\,mol^{-1}}$ [14]

pressure chemical reactor systems. Further, while being suitable for long term storage and clearly usable for automotive-applications [13, 15], the role of long-chained alkanes and alcohols for short-term energy cycling is questionable.

1.1 Catalysis for energy applications

The Sabatier reaction (equation (1.2)) was originally developed for removal of carbon oxides from hydrogen streams but has gained renewed interest in recent times thanks to the methane (CH_4) product that is an attractive energy carrier[4] [12].

$$CO_2 + 4\,H_2 \longrightarrow CH_4 + 2\,H_2O \tag{1.2}$$

Although CH_4 has lower energy density compared to long-chain alkanes and alcohols, its ease of production makes it suitable for intermediate storage times and short-term energy cycling [17]. Furthermore, it can be utilised in current technologies developed for natural gas in regards to transport and usage, thus decreasing the implementation cost. Despite the fact that a chemical reaction might be energetically favoured, that alone may not warrant it being plausible. Take as an example diamonds. While De Beers slogan is *a diamond is forever* they are in fact unstable and degrade slowly forming graphite ($\Delta G_f^\circ = -2.9\,\mathrm{kJ\,mol^{-1}}$ [18]). Fortunately, the degradation time amounts to billions of years, and as such you do not need to worry about your engagement ring slowly turning into a decorative pencil. This is because the degradation reaction is (strongly) kinetically limited, i.e., the reaction rate is sluggish, which is a characteristic that many industrially relevant reactions share. To speed up the kinetics one may, for example, heat up the sample because the rate of chemical reactions increase with increased temperature. The downside with heating is that it will not only increase the running cost of the reaction but might also open up for unwanted side reactions lowering the desired reaction selectivity. A fascinating approach to circumvent this problem is the usage of a catalyst. While the catalyst can not change the free energy of a reaction, i.e. a thermodynamically impossible reaction remains impossible, it can greatly increase its rate towards equilibrium by providing an alternative reaction pathway [19, pp 1–4]. Analogously, one can envision the catalytic process as taking a shortcut. We still move from point A to B (potential energy change is the same) but use less energy intense steps to do so. A more formal description is depicted in Figure 1.1. Here E_a is the activation energy of the reaction, the energy needed for the reaction to occur, and I_x are the intermediary steps of the reaction.

4: In addition, some niche applications has arisen, such as the removal of CO_2 from air and recycling of H_2O, as done at the international space station [16].

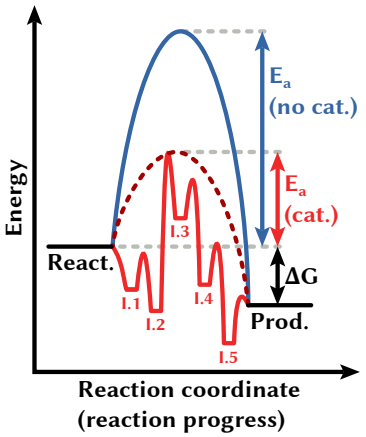

Figure 1.1: Schematic energy diagram for a reaction, showing the activation energy (E_a) for a non-catalysed reaction and a catalysed reaction. For the catalysed reaction, an apparent change in activation energy is shown as the dashed line whereas the full line shows the actual reaction with intermediary steps.

Like the shortcut, a catalyst is not consumed by its use. However, its shape and behaviour may change during the reaction cycle, but returns to the state of the initial step after completing the reaction cycle [19, pp 1–4].

1.2 Motivation of this work

The slow kinetics of catalysts for the Sabatier reaction makes high temperatures and pressures needed in order to gain industrially relevant yields [20, 21]. As such, the development of catalyst capable of operating close to ambient conditions would decrease the energy intensity of the process and open up for the methanation reaction to be run in less expensive industrial units and/or smaller remote apparatuses.

Background 2

2.1 The Sabatier reaction

During the turn of the 20th century, Paul Sabatier together with Jean-Baptiste Senderens discovered what is now known as the Sabatier reaction, shown in equation (2.1), for which Sabatier was awarded the Nobel prize in chemistry in 1912 [22]. While originally utilised for purification of gaseous hydrogen from carbon oxides, it has now gained a renewed interest due to applications such as fuel production, energy storage and oxygen recycling [12].

$$\begin{aligned} CO_2(g) + 4\,H_2(g) &\longrightarrow CH_4(g) + 2\,H_2O(g) \\ \Delta H_{298\,K} &= -165\,\mathrm{kJ\,mol^{-1}} \end{aligned} \tag{2.1}$$

The reaction is strongly exothermic and the drop in entropy limits the maximum conversion of the Sabatier reaction at atmospheric pressure, unless carried out at low temperatures. As such, industrially elevated temperature and pressure is utilised in order to achieve fast kinetics and to avoid the limitation to the maximum conversion [20, 21]. In regards to energy usage[1] and simplicity of equipment, a low temperature and pressure solution might be more suitable. For heterogeneous catalysts operating at atmospheric conditions, initial activity at temperatures as low as 200 °C and operable temperatures (high conversion) as low as 300 °C are not uncommon for methanation catalysts [23, 24].

1: In addition to general industrial production, for some applications such as the previously noted air purification at the international space station [12], more complex systems such as those employing elevated pressures might be unsuited.

Ever since the days of Sabatier, methanation catalyst are predominantly composed of nickel, most often deposited on high surface metal oxide supports [12, 21, 25]. While metals such as rhodium and ruthenium can surpass nickel in regards to activity, the high activity and selectivity together with much lower price makes nickel based catalysts so far more favourable [21, 24]. However, some aspects limit the nickel catalysts such as deactivation by oxidation and formation of volatile carbonyls at low temperatures (< 300 °C), and carbon deposition [12, 20, 21, 26, 27]. For these reasons, noble metals are still of interest in the pursuit of decreased reaction temperature for CO_2 methanation.

Proposed reaction mechanisms

While a black box approach of catalyst screening allows for the discovery of new well performing catalysts using also some chemical intuition, it can seldom provide the insight needed to finely tune the properties of the catalyst. In order to accomplish this, knowledge of the reaction mechanism is needed in order to, for example, determine the rate determining step of the reaction and the cause behind its limitation. For CO_2 methanation, as well as CO_2 hydrogenation in general, the reaction pathway is commonly following one of three different routes: the formate, carbon monoxide[2] and carboxylate pathway [12]. Among these, it is the carbon monoxide and formate routes that have been observed experimentally, see equations (2.2)-(2.7) [12, 25]. For the traditional Ni catalysts, *e.g.*, Ni/SiO_2, Ni/Al_2O_3 and the like, which have enjoyed an extensive amount of studies, the carbide pathway in which the CO dissociates and forms elementary carbon (C) that is further hydrogenated into CH_4 is the most commonly attributed pathway [12, 21, 25]. However, while proceeding by a carbon monoxide based pathway, the intermediary steps of the nickel based catalysts have been shown to be dependent on the support. As an example, an IR study of a Ni/ZrO_2 catalyst where the ZrO_2 is an active support, intermediary bicarbonates and formates were observed, see equations (2.14)-(2.16) [25]. As such, while studying the reaction mechanism one may encounter an interplay between pathways as well as red herrings as the observation of intermediates most commonly associated to certain pathways might lead to the conclusion that the reaction follows that particular pathway.

One property that is often tuned, by example choice of support, promoter and active material, is the adsorption strength of the reactants towards the catalyst. According to Sabatier's principle, adsorbates may not adsorb too strongly, as they then will not desorb, nor too weakly, as not enough accumulation of adsorbates occur and the adsorption is too weak for dissociation [19].

2: Also called the reverse water-gas shift (rWGS) or carbide pathway, based on pre- and succeeding steps.

Reaction steps of the carbide pathway [25].

$$CO_2 + H_2 + * \rightarrow CO^* + H_2O \quad (2.2)$$
$$CO^* + H_2 \rightarrow C^* + H_2O \quad (2.3)$$
$$C^* + H^* \rightarrow CH^* + * \quad (2.4)$$
$$CH^* + H^* \rightarrow CH_2{}^* + * \quad (2.5)$$
$$CH_2{}^* + H^* \rightarrow CH_3{}^* + * \quad (2.6)$$
$$CH_3{}^* + H^* \rightarrow CH_4 + 2* \quad (2.7)$$

$*$ Empty adsorption site
i^* Adsorbed i

Reaction steps of the formate pathway as shown in the review by Vogt et al. [12].

$$CO_2 + H^* \rightarrow HCOO^* \quad (2.8)$$
$$HCO^* + H^* \rightarrow H_2CO^* + * \quad (2.9)$$
$$H_2CO^* + H^* \rightarrow H_2COH^* \quad (2.10)$$
$$H_2COH^* + H^* \rightarrow CH_2{}^* + * \quad (2.11)$$
$$CH_2{}^* + H^* \rightarrow CH_3{}^* + * \quad (2.12)$$
$$CH_3{}^* + H^* \rightarrow CH_4 + 2* \quad (2.13)$$

However, as this pathway typically involves a metal oxide, several additional potential reaction steps can be imagined such as the formation of a methoxy group (CH_3O^-). This would then be similar to proposed formate pathways for other hydrogenation catalysts, such as those for CO_2 into methanol [28]. If so, tuning the characteristics of the catalyst may open the possibility of producing other products.

$$CO_2 + OH^{-,*} \longrightarrow HCO_3{}^{-,*} \quad (2.14)$$
$$HCO_3{}^{-,*} + H_2 \longrightarrow HCOO^{-,*} + H_2O \quad (2.15)$$
$$HCOO^{-,*} + * \rightleftharpoons CO^* + OH^{-,*} \quad (2.16)$$

2.2 The importance of transient *in situ* studies to reveal reaction mechanisms

While both *ex situ* and *in situ* studies in regards to the surface reactions are often conducted with ease by the use of methods such as infrared spectroscopy (see Section 3.4), the behaviour of the catalyst material during the reaction is not as easily studied, often leaving it as an *ex situ* comparison of the fresh and spent material. Crucial information such as the restructuring of the catalyst during the reaction therefore go unnoticed. Furthermore, not only active species but also spectators, a species that is formed at reaction

conditions but does not participate in the (main) reaction [29], may be observed and falsely attributed as a true reaction intermediate. Additional factors must therefore be included as to separate the contributions of active and spectators species, for which transient studies are common. This is further discussed in some depth in Section 3.5.

2.3 Objectives

This thesis aims at providing fundamental understanding of the behaviour of the Rh/CeO_2 methanation catalyst under operation conditions and a first insight into the mechanistic pathway of the CO_2 methanation reaction over this type of catalyst.

Methodology 3

In this work, the *in situ* behaviour of the catalyst material and the surface reactions over the catalyst for the considered chemical reaction were studied. To accomplish this, the changes in crystal structure and oxidation state was studied using synchrotron X-ray sources (Section 3.2 and 3.3) and the adsorbates of the reaction was studied by infrared spectroscopy (Section 3.4). As both active, those that participate in the reaction, and spectators, those that do not participate in the reaction, are observed in the resulting data, these experiments were conducted transiently using a modulation excitation approach (Section 3.5) in order to remove the contribution of spectators from the data set.

3.1 Catalyst preparation 9
3.2 X-ray diffraction 10
3.3 X-ray photoelectron spectroscopy 11
3.4 Infrared spectroscopy . . . 11
Diffuse reflectance 12
Molecular vibrations and selection rules 13
3.5 Modulation excitation spectroscopy 13
Phase-sensitive detection 14

3.1 Catalyst preparation

One of the principle design rules for a heterogeneous (solid) catalyst to be efficient is that it should expose a high specific surface area (m^2/g) hosting the active sites or, as in the case of supported catalysts, carrying and stabilising the catalytically active particles [30][19, pp 167–169]. There are numerous ways of making catalysts, ranging from top-down approaches such as milling the active material into powder to bottom-up approaches with, for example, controlled and well defined nanoparticle synthesis and deposition [31–34]. Another common route that is simple, yet effective, is impregnation of a support material with a solution of a precursor material, which gives small and well dispersed nanoparticles on that support [32]. The impregnation can be made in different ways. The simplest form of wet impregnation uses an excess of precursor solution and the remaining liquid is evaporated by applying heat. The procedure may result in large particles and clogging of the pores of the support material, which decreases the material utilization and influences the catalytic properties of the catalyst. An alternative route is the dry impregnation, also called incipient wetness impregnation or capillary impregnation [32]. The support material is impregnated with a liquid volume just enough to fill the pores. The sample is then frozen and freeze-dried as to remove the solvent by sublimation. This way, the problems of wet impregnation are avoided as the precursor is immobilised and largely not affected by drag forces by the solvent during removal [32].

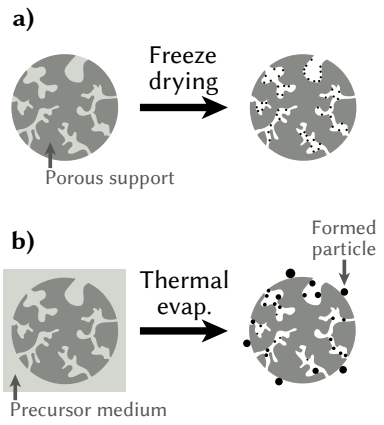

Figure 3.1: Illustration showing the start and end state of impregnation performed as dry (a) and one with excess of solvent and thermally dried (b). For the thermally dried sample, the formation of large particles, localised at pore openings and clogging pore channels may occur.

In this thesis, the ceria supported rhodium (Rh/CeO_2) catalysts were prepared by incipient wetness impregnation, using $Rh(NO_3)_3$ (Paper I) or Rh dissolved in nitric acid (Paper II) as Rh precursor.

3.2 X-ray diffraction

A well known optical phenomenon is the bending of light when it passes through slits of size similar to or less than its wavelength. The concept is referred to as diffraction and can be used to determine the crystal structure of a material [35], which can be thought of as planes of atoms forming an infinite number of repeating slits. As typical inter-atomic distances are in the Ångström scale, X-rays provide the suitable wavelength to perform the experiment. The mathematical model for the description of the diffraction angle (θ) in regards to the inter-planar distance (d) and wavelength (λ) was first presented by Bragg in 1913 [36]. The corresponding equation is referred to as the Bragg's law and can be seen in equation (3.1) and a schematic representation of the process can be seen in Figure 3.2 [35].

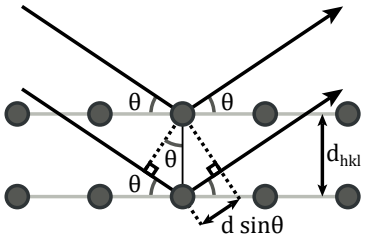

Figure 3.2: Schematic representation of Bragg's law. Individual atoms are shown as balls and lines highlighting the crystal plane have been added. Note that the two shown scattered photons share angle and will constructively interfere, providing a defined maximum intensity. Furthermore, the extra distance for the lower photon gives rise to the $2d\sin(\theta)$ in Bragg's law.

$$2d\sin(\theta) = n\lambda \tag{3.1}$$

Upon making a diffraction experiment, the obtained data is typically presented as a diffractogram, i.e., the measured intensity of the diffracted light against its corresponding diffraction angle as 2θ. As the angle of diffraction in equation (3.1) is wavelength dependent, one cannot directly compare diffractograms produced by different X-ray sources. In order to circumvent this problem, one may move from the R-space expression to the q-space, expressing it as a relation between the diffraction angle and wavelength, see equation (3.2).

$$q = \frac{4\pi}{\lambda}\sin(\theta) = \frac{2\pi}{d} \tag{3.2}$$

The diffraction caused by a perfect single crystal, which has a defined orientation, results in discrete and clear diffraction spots [35]. For powder samples, ring patterns are instead produced due to the random orientation of the crystals in the analyzed powder [35]. Nevertheless, the diffraction angle is still the same.

In this study, the catalyst was studied by high energy X-ray diffraction (HE-XRD) with a high photon flux by the use of synchrotron light. The high energy and photon flux allowed for a detailed transient *in situ* study, which is prohibited by conventional lab X-ray sources.

3.3 X-ray photoelectron spectroscopy

The discovery of the photoelectric effect [37], the emission of (most commonly) an electron following the absorption of electromagnetic radiation, have lead to numerous different applications out of which X-ray photoelectron spectroscopy is one which is crucial in the field of catalysis research [19]. By measuring the kinetic energy of the ejected photoelectron one can find the original binding energy of said electron by equation (3.3), given that the energy of the X-ray photon ($h\nu$) and work function of the instrument (ϕ) is known [19]. This process is illustrated in Figure 3.3.

$$E_{\text{binding}} = h\nu - E_{\text{kinetic}} + \phi \tag{3.3}$$

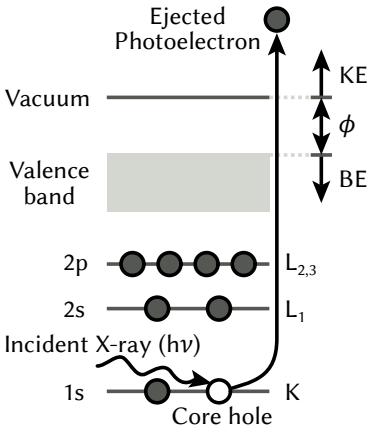

Figure 3.3: A schematic figure showing the ejection of a photoelectron from the 1s orbital of oxygen by an X-ray photon. KE refers to the kinetic energy whereas BE is the binding energy. ϕ is the work function of the instrument.

This binding energy can not only reveal the kind of atoms present in the sample, but effects such as shifts of its peak in the spectrum may also provide an insight into its oxidation state.

Typically, XPS is limited to pressures $\leq 10^{-6}$ mbar due limitations to the path length of the emitted photoelectron by inelastic scattering by the surrounding gas phase [38]. As such, *in situ* studies by XPS have been severely limited in regards to catalysis studies. In more recent years, ambient pressure XPS (AP-XPS) in which the gas pressure of the sample cell is close to atmospheric condition have become possible thanks to sophisticated instrumental setup and high photon flux, supplied by synchrotron sources [38–40].

In this study, the oxidation state of the catalyst as well as the formation of some adsorbates formed was studied during CO_2 methanation by the use of AP-XPS.

3.4 Infrared spectroscopy

Infrared spectroscopy is a characterisation technique used to distinguish between different materials and to determine some of its constituents by measuring the IR absorption of the material. Unlike absorption of more energetic light, such as visible light, infrared light typically has a too low energy as to cause electronic transitions but instead suitably can excite vibrational states [41]. As such, IR light can be used to distinguish between different functional groups of a material based on their different absorption at different wavelengths. For absorption spectroscopy, it is foremost the transmission (T) and reflection (R) that is taken into regard whereas scattering effects are neglected. The quantitative expression of transmission spectroscopy follows equation (3.4) [41, 42]:

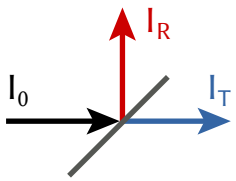

Figure 3.4: Schematic representation of transmission and reflectance

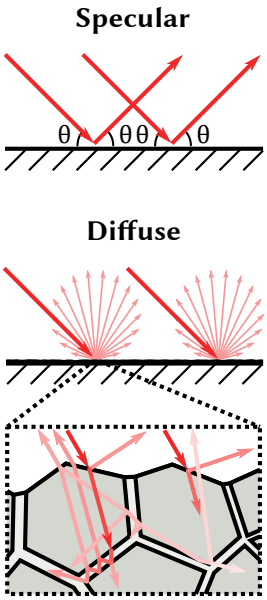

Figure 3.5: Schematic illustration for the difference between specular and diffusive reflection. The "zoom" is an example of some internal reflections of a polycrystalline material.

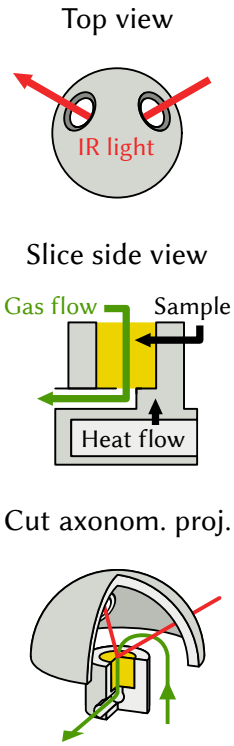

Figure 3.6: Schematic illustration of the DRIFTS cell set-up, showing the dome and sample cup without surrounding enclosure.

$$T = \frac{I_0}{I_T} \tag{3.4}$$

where the intensity of the incident light (I_0) is divided by the intensity of the transmitted (I_T) light. In the case of a reflection measurement the intensity of the reflected (I_R) light replaces I_T in equation (3.4). The absorption of the light is expressed as absorbance (A), which is either the logarithm of the reciprocal transmission or reflectance of the light as expressed by equation (3.5) for transmission.

$$A = \log_{10} \frac{1}{T} \tag{3.5}$$

When measuring the absorbance, typically either transmission or reflectance is accounted for and in the case of a reflectance measurement, the absorbance is often referred to as a pseudo-absorbance.

Diffuse reflectance

There are two kinds of reflections, the specular and diffuse reflection out of which it is perhaps specular reflection that comes to ones mind when thinking about reflection of light. Specular reflection is the mirror-like reflection. For specular reflection, the light is reflected at the same angle as the incident light in regards to the normal, giving a mirror-like or glossy appearance. This kind of reflection occurs for finely ordered materials such as larger single crystals but also flat and smooth materials such as metals and glasses. In contrast to this, diffuse reflection produces, as its name suggests, a more randomly distributed reflection. While the light is reflected at the same angle as the incident light (in regards to the norm) like the case of specular reflection, the incident rays do not share a common norm due to the polycrystalline structure and/or the roughness of the surface that creates a multitude of different reflection angles in regards to the average norm [42].

In contrast to transmission and specular reflection experiments, diffuse reflectance can easily be performed on a powder sample without any sample preparation as the phenomena that often plagues these two methods is instead the point of interest – the diffuse reflection.

Molecular vibrations and selection rules

While absorption of visible and ultraviolet light typically leads to electronic transitions, i.e., one or more electrons absorb the light and achieve a more energetic state, IR light can rarely produce electronic transitions but instead induce vibrations in the absorbing molecule. The energy for the promotion of this vibration is based on factors such as binding energies and bond angles, which can be realised by visualising the molecule as a harmonic oscillator [41, 43].

However, not all kinds of groups can be observed by IR spectroscopy due to selection rules. While it's only possible for a material to absorb visible light if the energy of the photon corresponds to the energy gap between the electronic states, IR light has an extra criteria that origins from the molecular structure of the probed material. In order for a molecule to absorb light, the resulting vibration needs to induce a net change in the dipolar moment [43]. Take for example CO_2, there are two different possible stretchings, the symmetric and asymmetric stretching of the C=O bonds. While the symmetric stretch causes a change in the dipole moment for each isolated bond, there is no net change due to the two stretchings counteracting one another. Whereas for the asymmetric stretching, the two C=O vibrations change the dipole moment in the same direction, thus adding their contributions to a net change.

Table 3.1: The six normal modes of vibration, applied to the CO_2 molecule, with the net change in dipole moment, $\Sigma\vec{\mu}_i$. Note that of these 6 vibrations only 4 are observed for CO_2 as ρ and τ are rotations for CO_2 and ν_s is IR inactive due to lack of net change in dipole moment.

Stretching		Bending			
		In-plane		Out-of-plane	
ν_s (Symmetric)	ν_{as} (Asymmetric)	δ (Scissoring)	ρ (Rocking)	ω (Wagging)	τ (Twisting)
	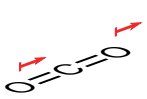	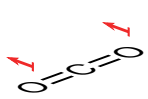		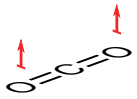	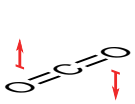
$\Sigma\vec{\mu}_i = 0$	$\Sigma\vec{\mu}_i > 0$	$\Sigma\vec{\mu}_i > 0$	$\Sigma\vec{\mu}_i = 0$	$\Sigma\vec{\mu}_i > 0$	$\Sigma\vec{\mu}_i = 0$

3.5 Modulation excitation spectroscopy

One of the greatest challenges when to determine the reaction pathway for a given reaction and catalyst is to distinguish true intermediates from spectators species that form during the reaction but not take part in the main reaction. One commonly utilised experimental design as to resolve this problem is the *modulation*

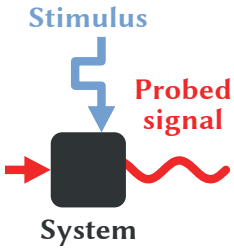

Figure 3.7: A conceptual sketch of a MES experiment. Behaviour and content of the system which otherwise would be hidden can be determined indirectly by studying its response to a stimulating signal.

excitation approach. In this kind of experiment, a parameter that is controlling the behaviour of the system under study is changed, which results in a response by the system [44]. An example of this could be the perturbation of a reaction from its steady-state by switching on/off the flow of one of the reactants, which results in a change of concentrations in the product flow and/or the coverage for different adsorbates on the catalyst. A species responding to this modulation thus shows a dependence on the concentration of the reactant and is therefore likely an intermediate of the studied reaction or a side reaction. By rapidly changing the modulation parameter, the response of slow side-processes can be hampered. If the response of the system remains repeatable throughout the pulses (no deviations), accumulation and averaging of the responses in the series is meaningful as both a high time resolution and improved signal-to-noise are gained.

As an example, consider the hypothetical reaction $A + B_2 \longrightarrow E$ that is heterogeneously catalysed (solid catalyst, gaseous reactants). The intermediary reaction steps are given by equation (3.6) to (3.10). In addition to these reactions, both a rapid and a slow side reaction occur as expressed by equation (3.11) and (3.12), respectively. In order to simplify the model, assumptions are made that include no presence of mass transport limitations, all the reactions occur on an extended flat surface and all adsorbate species except A′ are adsorbed on the same type of adsorption site. By applying a modulation in the form of sinusoidal change of the partial pressure of A (p_A) on this reaction system while keeping the partial pressure of B constant, a response similar to that shown in Figure 3.8 can be obtained. While initially showing a response to the stimulus, the side reaction (3.12) eventually reaches steady-state due to its slow kinetics. This kind of response might be expected from stable, non-interactive, species such as carbonates and hydroxides. While these can be easily filtered out by the modulation excitation spectroscopy (MES) approach, rapid reactions such as (3.11) may still show a response. A relevant example to this work would be the equilibrium reaction $HCOO \rightleftharpoons CO + OH$.

Reaction steps of the simulated reaction

$$A + * \rightleftharpoons A^* \tag{3.6}$$
$$B_2 + 2* \rightleftharpoons 2\,B^* \tag{3.7}$$
$$A^* + B^* \rightleftharpoons C^* + * \tag{3.8}$$
$$C^* + B^* \rightleftharpoons E^* + * \tag{3.9}$$
$$E^* \longrightarrow E + * \tag{3.10}$$
$$A^* + B^* \rightleftharpoons D^* + * \tag{3.11}$$
$$A^* \rightleftharpoons A'^* \tag{3.12}$$

$*$ Empty adsorption site
i^* Adsorbed i

$$\theta_i = \frac{\text{Nr of sites occupied by } i}{\text{Total amount of sites}} \tag{3.13}$$

Phase-sensitive detection

For data obtained from modulation excitation measurements, removal of the static signal and extraction of the delay for the responding signal compared to the modulation is a main target. In order to accomplish this, so-called phase sensitive detection (PSD) can be applied, either by Fourier transform or, as in this study, by a lock-in amplifier, expressed in regards to a transient IR data set in equation (3.14) [45]. In equation (3.14), the $A(\tilde{\nu}, t)$ term is the amplitude in the time-domain, $k\omega^1$ is the analysed frequency, τ is

1: For which $k = 1$ corresponds to the fundamental vibration, $k = 2$ is the first harmonic and so on

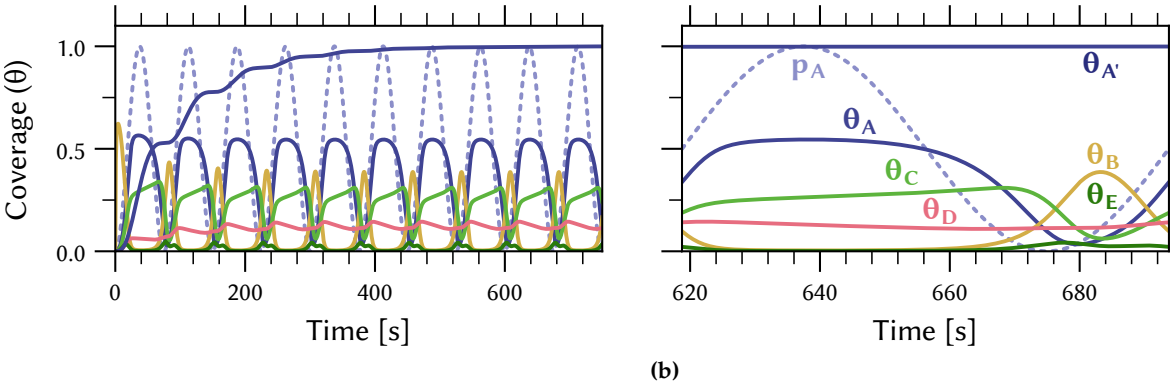

Figure 3.8: Simulated ME experiment in which a primary reaction is sinusoidally modulated. In a), the reaction initiation followed by multiple modulation steps are shown. A single period after the system has reached a constant oscillation is shown in b).

the period time, ϕ_k^{PSD} is the operator controlled phase angle and $A^{\phi^{\mathrm{PSD}}}$ is the phase-resolved amplitudal data.

$$A_k^{\phi^{\mathrm{PSD}}}(\tilde{\nu}) = \frac{2}{\tau}\int_0^{\tau} A(\tilde{\nu},t)\sin(k\omega t + \phi_k^{\mathrm{PSD}})dt \tag{3.14}$$

By application of equation (3.14) to MES data, signals that do not show a periodic response to the stimulus, such as noise and spectators, are reduced or fully cancelled out [46] and integration over additional periods further increases the signal-to-noise ratio. As an example, solving this on the previous simulated MES example (Figure 3.8) for the full phase period ($0° \leq \phi_k^{\mathrm{PSD}} \leq 360°$) with the same frequency as the p_{A} modulation results in Figure 3.9.

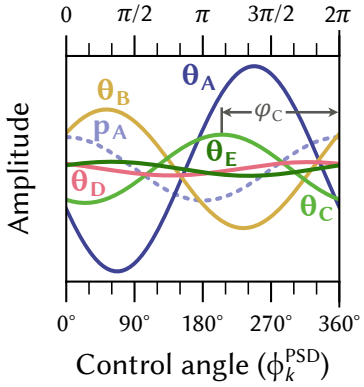

Figure 3.9: The phase resolved data of the simulated MES experiment, shown in Figure 3.8, solved for $k = 1$.

By finding the phase delay φ_k, i.e. how much out-of-phase the response is to the stimulus, one may sequence the order of events in a data set of multiple responses [47]. This phase delay can be obtained from the in-phase ($\phi_k^{\mathrm{PSD}} = 0°$) and out-of-phase ($\phi_k^{\mathrm{PSD}} = 90°$) amplitudes, as shown in (3.15) and (3.16) [45]. Solving the phase delays for the simulated example, one obtains a $|\varphi_k|$ order of D<A<C<E<B, providing the correct reaction sequence (A $\longrightarrow$ C $\longrightarrow$ E).

$$A_k(\tilde{\nu}) = \sqrt{A_k^{0°}(\tilde{\nu})^2 + A_k^{90°}(\tilde{\nu})^2} \tag{3.15}$$

$$\cos\varphi_k = \frac{A_k^{0°}(\tilde{\nu})}{A_k} \quad , \quad \sin\varphi_k = \frac{A_k^{90°}(\tilde{\nu})}{A_k} \tag{3.16}$$

As a square wave function may be expressed as a sum of infinite odd numbered harmonics (equation (3.17), Figure 3.10) one may study several frequencies[2] from a single square wave MES experiment, given the corrections shown in equation (3.18) and (3.19) [47].

2: Note that the Nyquist-Shannon theorem still limits the highest studiable frequency to half the sampling frequency

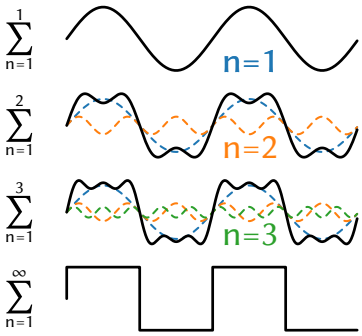

Figure 3.10: An illustration of how a square wave is constructed by the use of an infinite number of sinusoidal functions.

$$x(t) = \frac{4}{\pi}\sum_{n=1}^{\infty}\frac{\sin[(2n-1)\omega t]}{2n-1} \tag{3.17}$$

$$\frac{\pi}{4}(2n-1)A_{2n-1}^{SW} = A^{\sin}|_{\omega'=(2n-1)\omega} \tag{3.18}$$

$$\varphi_{2n-1}^{SW} = \varphi^{\sin}|_{\omega'=(2n-1)\omega} \tag{3.19}$$

In this thesis MES-PSD has been employed to remove spectator signals from IR characterisation of adsorbates during *in situ* CO_2 methanation over Rh/CeO_2. Furthermore, by analysing phase delays, some proposals of reaction mechanisms are given.

Results and discussion 4

4.1 Physico-chemical behaviour of the catalyst 17
Observing the crystal structural dynamics 17
Changes in the surface oxidation state 18
4.2 Exploring the surface reactions 18
Active and inactive, adsorbates at steady-state . . . 19
Active species – to separate the wheat from the chaff . . 20
4.3 Reaction mechanisms – formulating an idea 24

In regards to the study of the function of a catalyst, there are two interlinking aspects to consider — the behaviour of the catalyst material, and the surface reaction. In Paper I, we explored the change in crystal structure and oxidation state of the catalyst as well as formation of surface adsorbates. Due to some ambiguities regarding the adsorbates, a more in depth study focused solely on the surface reaction was performed in Paper II. In these studies, the catalyst was studied in the temperature span of 200-350 °C. The importance of this span, as reported in a previous kinetic study [48], is the initiation of CO (g) formation at temperatures between 250 and 350 °C whereas CH_4 (g) production occurs in the entire temperature interval.

4.1 Physico-chemical behaviour of the catalyst

In order to probe for the possibility of formation of new catalyst compounds during the reaction, such as oxides and carbides of the active metal, high-energy X-ray diffraction (HE-XRD) was performed. By this method the bulk phases of material domains with sufficient long range order can be studied *in situ*. Further, ambient pressure X-ray photoelectron spectroscopy (AP-XPS) was performed in order to observe changes in oxidation state of the surface *in situ* upon exposure to reaction atmospheres.

Observing the crystal structural dynamics

The crystal structural dynamics of the Rh/CeO_2 catalyst was studied by transient *in situ* HE-XRD using a modulation excitation approach (see Section 3.5). While the sample was exposed to a constant CO_2 flow (0.5 vol.%), the H_2 concentration was periodically changed between 0 and 2 vol.% in a square-wave fashion (20 min period time) while the diffractogram of the sample was recorded. The resulting diffractograms can be seen as difference plots in Figure 4.2. While weak, a peak corresponding to supported rhodium metal ($Rh_{supp.}$) is observed during these experiments. This reflection corresponds to a *d* spacing of 2.2 Å, whereas 2.1 Å is expected for metallic Rh, which is likely due to a strong interaction with CeO_2 and possibly also with a boundary RhO_x phase as observed with AP-XPS (below). As for the lack of strong rhodium

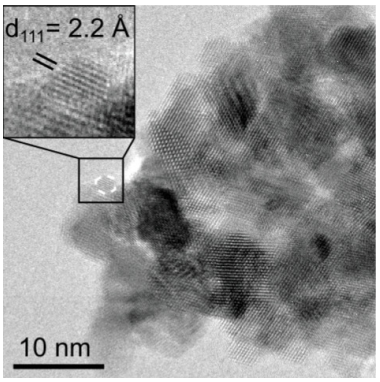

Figure 4.1: High-resolution TEM image of the Rh/CeO_2 catalyst used in the *in situ* structural study. The inset shows a 2 nm Rh crystallite, showing the 2.2 Å interplanar distance of the (111) plane.

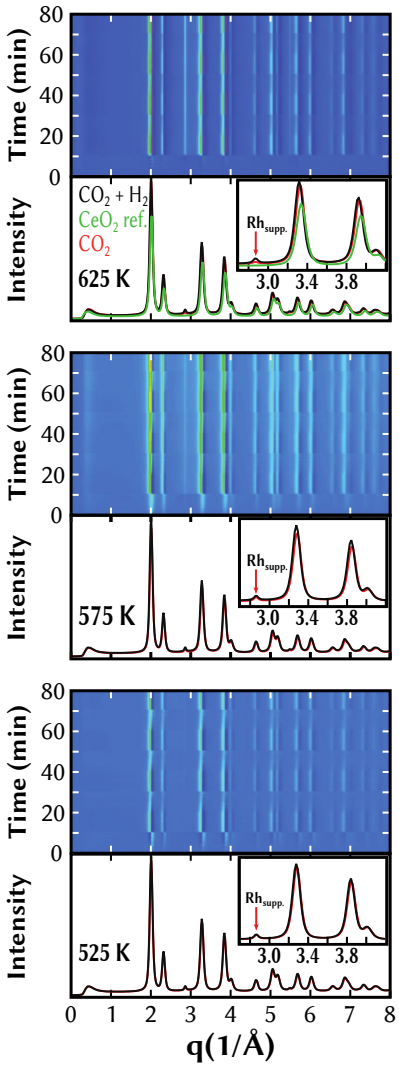

Figure 4.2: X-ray diffratograms of Rh/CeO_2 during CO_2 hydrogenation with H_2 pulses with an inset showing the peak of $Rh_{supp.}$. In the contour plot, the initial pattern has been subtracted from the series.

peaks, this is likely due to a combination of amorphous rhodium metal and small particles (of which particle diameters of 2-3 nm were primarily observed in TEM and the average was 4 nm), for which both of these factors create a lack of well defined long range order. While no change in regards to rhodium is observed during this experiment, a decrease in q for the reflections of CeO_2 during CO_2 hydrogenation could be clearly seen. This decrease in q corresponds to an increase in interplanar distances (d), which in turn suggests an expansion of the unit cell. While this reduction is expected, the partial re-oxidation of CeO_2 following the removal of H_2 (increase in q) from the gas stream provides a new insight to the reaction. Namely, it suggests that either CO_2 itself or remaining reaction intermediate(s) from the hydrogenation reaction to some extent heals the oxygen vacancies formed at CeO_2. This shows that the redox behaviour of CeO_2 could be involved in the catalytic reaction mechanism, its role in the CO_2 methanation and rWGS reactions cannot be determined from this experiment alone.

Changes in the surface oxidation state

The oxidation state of the catalyst surface was explored using AP-XPS. As seen in Figure 4.3, both RhO_x and Rh metal phases with alternating ratios of the oxidised and reduced state are observed when the Rh/CeO_2 sample held at 595 K is exposed to a hydrogen (1.33×10^{-6} hPa) and oxygen (1.33×10^{-5} hPa) environment, respectively. Furthermore, the rhodium is not fully reduced under the hydrogen conditions. Similar to what is observed in the HE-XRD measurements, a partial reduction of CeO_2 is seen in the reducing environment as a decline of Ce^{4+} signal.

As for *in situ* study of the methanation using AP-XPS, a transient study was performed in which the sample was exposed to a gas mixture of 0.0133 hPa CO_2 and 0.1867 hPa H_2 and the temperature was gradually increased from 515 to 625 K. Like the previous reduction-oxidation experiment, rhodium remains as partially oxidised during the experiment. As for the C 1s region, formation of surface species such as HCOO and CO is seen. While present on the surface at 515 K, no CO (g) was detected by the mass spectrometer while CH_4 production was seen during the whole temperature range. The first CO (g) could not be observed until 615 K was reached.

4.2 Exploring the surface reactions

While the previous AP-XPS results show that CO and HCOO species form on the Rh/CeO_2 catalyst, the possibility of them

being intermediates could not be ascertained. As such, this was followed by a study focused solely on the surface reactions by the use of diffuse reflectance infrared Fourier transform spectroscopy (DRIFTS). An initial assessment of the surface adsorbates during reaction conditions was performed by steady-state hydrogenation at 200, 250 and 300 °C. Afterwards, the hydrogenation was studied transiently at the same temperature in order to deduce which of the adsorbates that correspond to intermediates.

Active and inactive, adsorbates at steady-state

After exposing Rh/CeO_2 to a flow of 0.5 vol.% CO_2, carbonate (CO_3) formation is observed out of which bidentate (b-CO_3) is the primary mode of adsorption of CO_2 to CeO_2, see Figure 4.5a. After the introduction of 2 vol.% H_2 to the CO_2 stream, additional peaks with high absorption appeared. Based on that these peaks correspond to hydrogenation products and the previous observation of HCOO in the AP-XPS experiment, one would expect that the peaks in the 1600-1300 cm^{-1} would correspond at least partially to HCOO. However, although C−H vibrations for HCOO are weaker than those of O−C−O, the weak C−H vibrations in the 2900-2800 cm^{-1} region signifies that HCOO only constitutes a minor portion of the peaks in the 1600-1300 cm^{-1} region. As for the prominent peak at 1744 cm^{-1}, its high wavenumber suggests a carbonyl such as a bridged CO which is further supported by its temperature dependence, coinciding with the rWGS. While showing some discrepancy (reference value: 1725 cm^{-1} [49]) to previous assignments, this peak is likely primarily composed of CO located at the interface of Rh and CeO_2 ($\nu_{Rh\text{-}CeO_2}$(C=O)). As for the mode of coordination, it has been suggested that the CO adopts a Rh−C=O−Ce coordination in which the oxygen is coordinated to a Lewis acid site of the support [49]. As for the higher wavenumber of this peak compared to the reference, this is possibly due to additional convoluted vibrations in the peak. Furthermore, minor peaks corresponding to species such as m-CO can be seen in the shoulder towards higher wavenumbers.

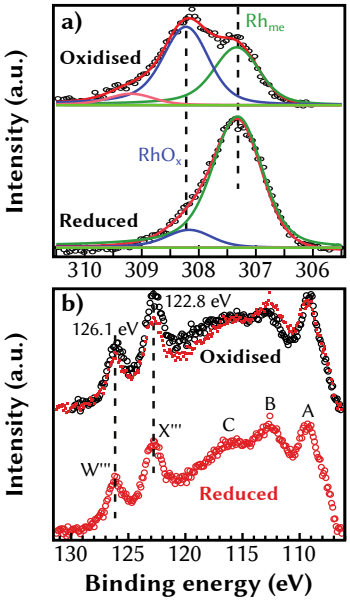

Figure 4.3: XPS spectra of Rh 3d (a) and Ce 4d (b) for reduced and oxidised Rh/CeO_2. Red squares in (b) is reduced Rh/CeO_2.

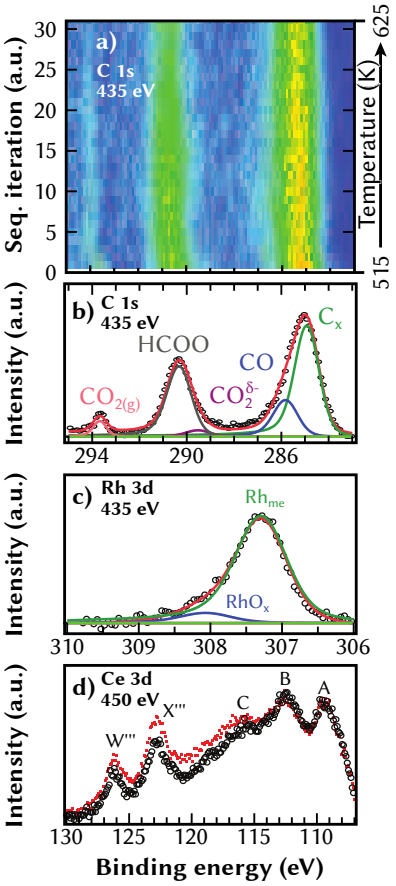

Figure 4.4: XPS spectra of Rh/CeO_2 during CO_2 methanation, showing C 1s during the temp. ramp (a) as well as C, Rh and Ce (b-d) at 515 K.

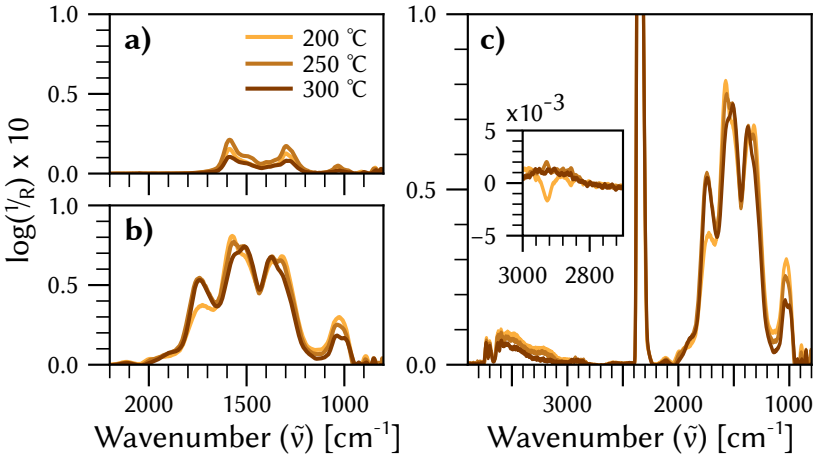

Figure 4.5: Steady-state *in situ* infrared spectra for the Rh/CeO_2 catalyst at the studied temperatures in the carbon-oxygen bond region 2200-800 cm^{-1} during (a) CO_2 adsorption (y_{CO_2} = 0.5) and (b) hydrogenation (y_{CO_2} = 0.5, y_{H_2} = 2) as well as the complete measured region with a zoom at the C-H bond region 3000-2550 cm^{-1} during hydrogenation (c).

Active species – to separate the wheat from the chaff

While providing an insight into the surface during reaction, it is difficult, if not impossible, to determine if an adsorbate is an intermediate or simply a spectator based on steady-state measurements. As such, in order to explore the possibility of these adsorbates being reaction intermediates, transient experiments with an modulation excitation approach were performed. Like the previous HE-XRD experiment, the CO_2 concentration in the gas flow was kept constant at 0.5 vol.% whereas the hydrogen concentration was modulated in a square wave fashion, alternating between 0 and 2 vol.%. However, unlike the HE-XRD, a higher sampling frequency (~2 Hz) and shorter modulation periods (τ) were employed in order to study the rapid reactions. Furthermore, both the modulation period (τ = 30, 60, 120 s) as well as temperature (T = 200, 250, 300 °C) were varied. As an example, the case of 300 °C with a modulation period of 120 s can be seen in Figure 4.6 with the gas modulation (a), the infrared spectra (b) and the difference infrared spectra (c). As seen in Figure 4.6c, clear response from vibrations in the carbonyl (2200-1700 cm^{-1}), carbonate (1700-800 cm^{-1}) as well as hydroxide and C–H (3800-2700 cm^{-1}) region were obtained. In regards to the other experiments, while the same regions showed a response, different intensities (both absolute and relative between the peaks) were obtained, for which high temperature and long periods favoured the carbonyl region in particular. Furthermore, steady-state condition was reached for several peaks at 120 s during H_2 flow. However, the hydrogenation products were never depleted during the H_2 purge steps. This is at least partially due to the dead volume of the reaction cell which prohibits a full purge of hydrogen from the gas phase during the modulation period. As such, one should take into account that the reaction is only perturbed by the modulation, not initiated and quenched.

In order to more easily compare the adherence of the response

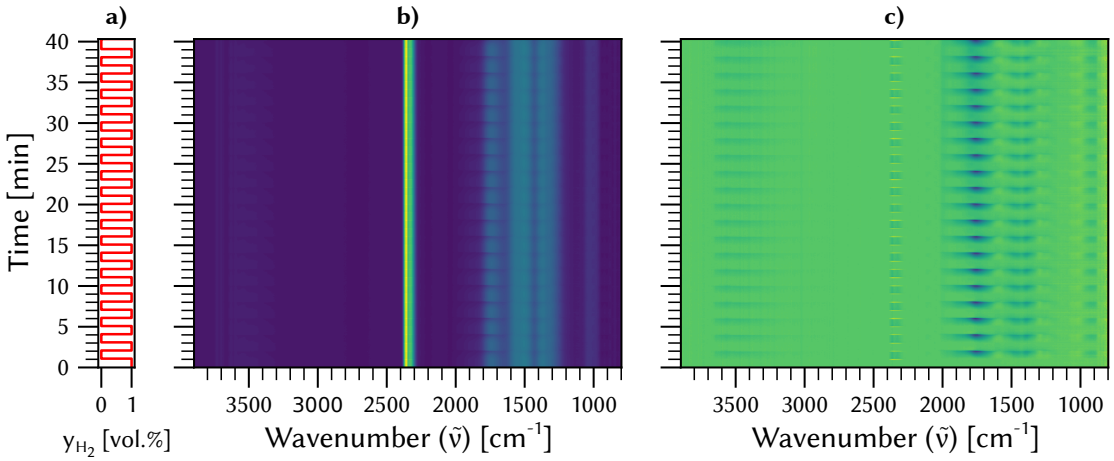

Figure 4.6: Modulation excitation spectroscopic measurement of CO_2 hydrogenation over a Rh/CeO_2 catalyst at 300 °C showing (a) the imposed H_2 concentration stimulus with period $\tau = 120$ s, (b) collected in situ infrared difference spectra and (c) in situ infrared difference spectra where the first difference spectrum has been subtracted from each difference spectrum in the full measured range 3900-800 cm^{-1}.

to the stimulus, remove static contributions as well as noise this time-resolved data was further analysed by phase sensitive detection (PSD), using a lock-in amplifier (see equation (3.14)) which was integrated over several periods. The obtained phase-resolved spectra ($A^{\phi^{\text{PSD}}}$) of the 2200-900 cm^{-1} region can be observed in the top rows of Figure 4.7 for modulation period 120 s (panel a), period 60 s (panel b), and period 30 s (panel c) between $0° \leq \theta^{\text{PSD}} \leq 180°$[1]. Furthermore, the bottoms rows shows a composite plot in which the maximum amplitude ($A^{\phi^{\text{PSD, max}}}$) is given at each wavenumber, given a full period of $0° \leq \theta^{\text{PSD}} \leq 360°$, together with the corresponding phase delay (φ) for the most pronounced peaks, marked with bullets (•).

1: The $180° \leq \theta^{\text{PSD}} \leq 360°$ interval is not included for clarity. However, they can still be visualised by taking into regard that it is simply the reflection of $0° \leq \theta^{\text{PSD}} \leq 180°$ across the $\tilde{\nu}$ axis.

Carbonyls

While minor peaks such as m-CO at 200 cm^{-1} are seen, it is the previously assigned $\nu_{\text{Rh-CeO}_2}$(C=O) vibration, from steady-state measurements, that is the most prominent peak in the MES-PSD results, given $\tau \geq 60$ s and $T \geq 250$ °C. However, while appearing as a single peak during steady-state, the MES-PSD results show that it consists of at least two separate peaks approximately located at 1700 and 1800 cm^{-1}. This is most noticeable in the $\phi^{\text{PSD, max}}(\tilde{\nu}, T = 200$ °C, $\tau = 60$ s) spectrum (Figure 4.7b). Furthermore, it is unlikely that these vibrations belong to the same molecule as they do not share a phase delay (i.e. they are not formed at the same time). Out of these, the peak at 1700 cm^{-1} is expected to correspond to the previously assigned $\nu_{\text{Rh-CeO}_2}$(C=O) vibration. As for the 1800 cm^{-1}, its low wavenumber makes it unlikely to correspond to a bridged CO (br-CO) and is instead likely to correspond to CO in a hollow or hollow-like site (h-CO)[50, 51]. While this convoluted peak is

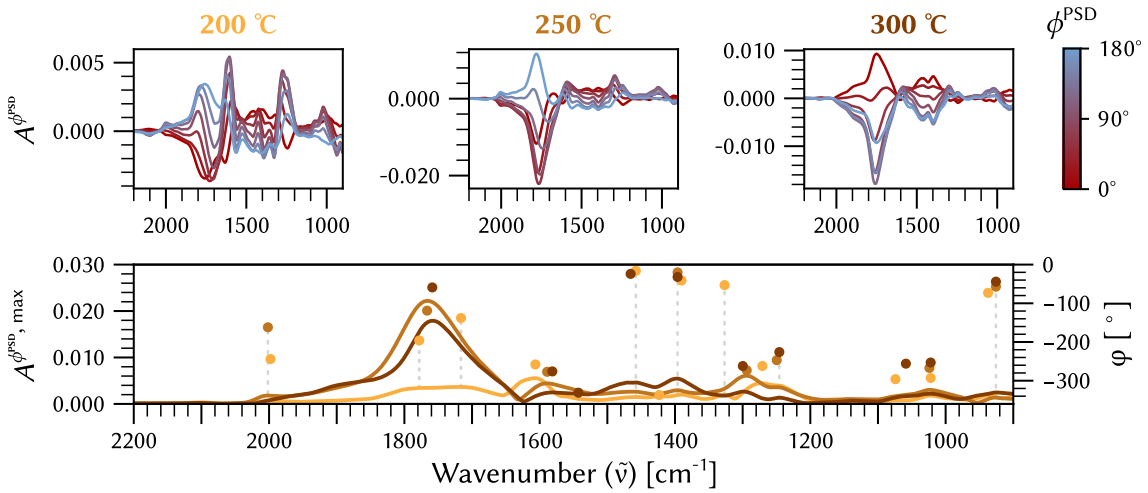

(a) Modulation period τ = 120 s

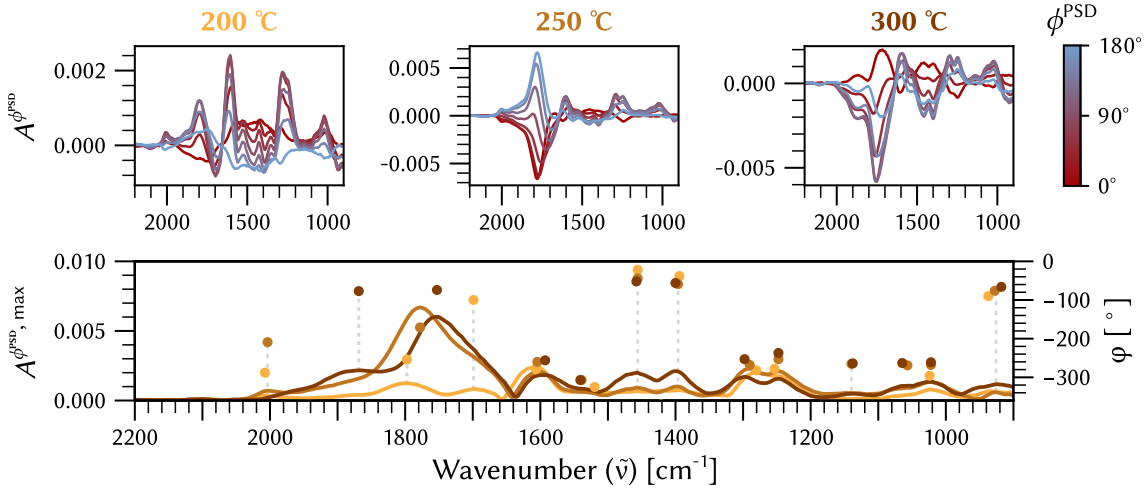

(b) Modulation period τ = 60 s

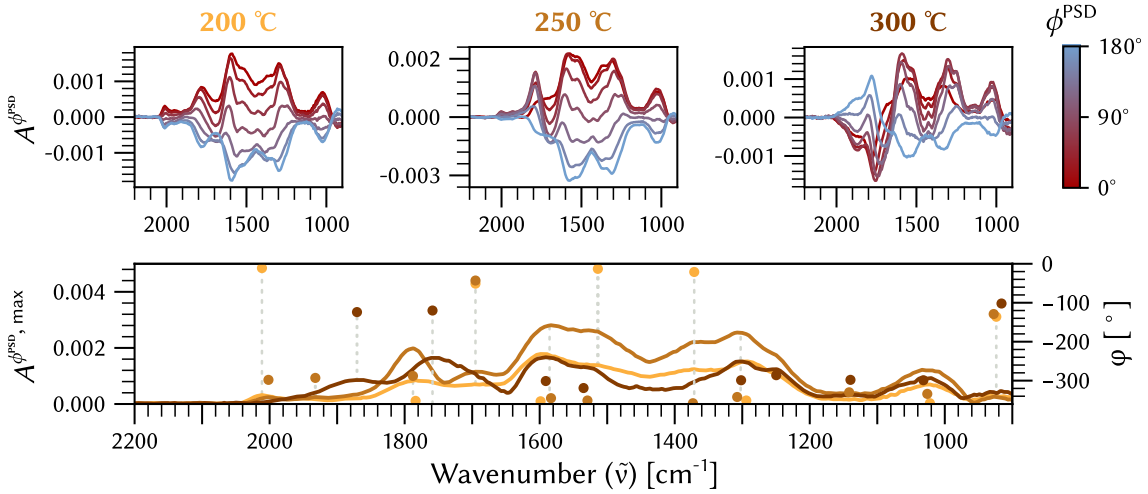

(c) Modulation period τ = 30 s

Figure 4.7: Graphical representation of phase sensitive detection (PSD) analysis results for CO_2 hydrogenation over Rh/CeO_2 at 200, 250 and 300 °C and different H_2 modulation period lengths (τ) of 120, 60 and 30 s. **Top rows:** PSD plots showing amplitude ($A^{\phi^{PSD}}$) versus wavenumber for demodulated spectra between $0° \leq \theta^{PSD} \leq 180°$. **Bottom rows:** Composite plots showing maximum amplitude ($A^{\phi^{PSD, max}}$) at each wavenumber in the period of $0° \leq \theta^{PSD} \leq 360°$ (**–**) together with the phase delay (φ) of the peaks (•) and visual guides (- - -).

primarily located close to the 1800 cm^{-1} peak, it shifts towards lower wavenumbers with increasing temperature. While a shift of the h-CO peak towards lower wavenumbers could be due to changes to its surrounding environment, perhaps a larger contributing factor is the increase of the CO_{RhCeO_2} to h-CO ratio. Furthermore, the intensity drop of these carbonyls, compared to other peaks in the spectra, at 300 °C coincides with the formation of CO (g) and bridged CO (br-CO, 1875 cm^{-1}). Although this decrease in h-CO could correspond to a potential increase in consumption rate of the hydrogenation reaction, it may also be due to a increase in desorption rate (giving a significant CO (g) formation) or a change in coordination to br-CO due to restructuring of the Rh surface. As for the relation between CO_{RhCeO_2} and h-CO, as CO_{RhCeO_2} the lower phase delay of CO_{RhCeO_2} opens up several different possibilities in regards reaction mechanisms. As an example, these carbonyls might be dependent on each other such as CO migration from the Rh-CeO_2 site to the extended Rh surface. As such, while the Rh surface alone should be able to dissociate oxygen from CO_2, the introduction of this new active site with faster kinetics could be linked to the promotional effect of CeO_2 to Rh. However, one need to take into account that CO_{RhCeO_2} and h-CO do not share adsorption site and possibly not active site either. Factors such as ratio of adsorption sites that participate in the reaction contra only facilitate migration as well as competition with other species in regards to surface coverage will have an effect. As such, this needs to be further explored in order to support or disregard this idea.

Table 4.1: Infrared peak assignments for the transient experiments in the 3000-2800, 2100-1700 and 1700-800 cm^{-1} region. The wavenumber values are approximated (±10 cm^{-1}) due to fluctuations during the time series and between the different experiments.

Species	$\tilde{\nu}$ [cm^{-1}]	Ref.
ν(C=O)		
$CO_{Rh\text{-}CeO_2}$	1700	[49]
h-CO	1800	[50]
br-CO	1875	[52]
m-CO	2010	[52]
p-CO_3		
ν_{as}(OCO)	1460	[53]
ν_{s}(OCO)	1390	[53]
b-CO_3		
ν_{as}(OCO)	1590	[54]
ν_{s}(OCO)	1280	[54]
b-HCOO		
ν_{as}(OCO)	1550	[55]
ν_{s}(OCO)	1300	[55]
ν(CH)	2850	[55]
δ(CH)	2950	[55]

Carbonates and formates

While formates are present on the catalyst, based on the O−C−O vibrations at 1550 and 1300 cm^{-1} as well as C−H vibrations at 2950 and 2850 cm^{-1} seen in Figure 4.7 and 4.8 [55], they do not exhibit a strong response to the hydrogen stimulus. However, as very minor responses might simply be due to experimental fluctuations, such as disturbances to the total flow during a gas switch, it is possible that this response does not originate from a participation in the methanation reaction.

Carbonates, which often are too stable to participate in hydrogenation do show a response to the hydrogen stimulus. One such carbonate is the b-CO_3 which was previously seen in the steady-state measurement. The b-CO_3 showed a huge phase delay to the modulation ($|\phi| > 180°$), signifying a consumption during hydrogen flow rather than production, as one would expect. However, another pair of vibrations are seen in the O−C−O region, those of 1460 and 1390 cm^{-1}, instead show a minute phase delay. One would therefore expect these to correspond to hydrogenation products,

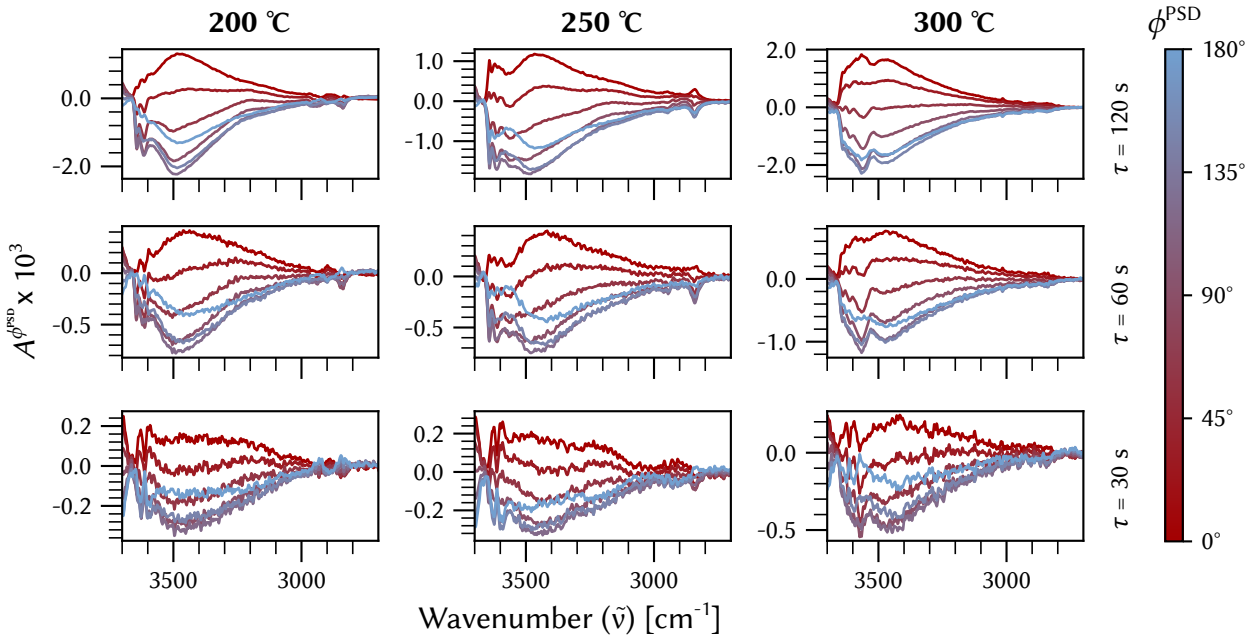

Figure 4.8: The phase resolved spectra in the region of 3700-2600 cm^{-1} of all MES-DRIFTS experiments. Peaks corresponding to C−H vibrations can be seen around 2950 (δ(CH)) and 2850 cm^{-1} (ν(CH)).

such as perhaps an inorganic carboxylate. However, the low ν_{as-s} split as well as the low wavenumber of the peaks makes this doubtful and they instead more likely correspond to polydentate carbonates. As the ceria surface reduces and restructures during the H_2 step, a p-CO_3 configuration might be more favourable for CO_2 adsorption rather than the previous b-CO_3 in the oxidised state. As such, the activity of these carbonates might therefore not be linked to the methanation reaction but are instead a response to the changes in the state of ceria. To gain an insight into the formation of p-CO_3, the phase delay of the carbonates was compared. By adjusting the the phase delay of b-CO_3 with half a period (ϕ(b-CO_3) + 180 ≈ - 80°), it is revealed that p-CO_3 has a shorter phase delay (-30°) and its formation should therefore be an earlier event than the b-CO_3 consumption. As such, the primary mode of formation for p-CO_3 should therefore be CO_2 adsorption rather than re-configuration of b-CO_3.

4.3 Reaction mechanisms – formulating an idea

While a multitude of different reaction pathways for CO_2 methanation over supported metal catalysts could be theorised, only a few pathways have shown a likelihood. Of these, it is primarily the formate and carbon monoxide routes, named after their primary reaction intermediates, which has been observed experimentally.

During reaction conditions, while a portion of the rhodium is oxidised its surface is expected to be reduced whereas both the

bulk and surface of ceria adopts a partially reduced structure. A number of active species in the form of carbonyls, carbonates and formates could be seen. These carbonyls were active even at low temperatures where CO (g) formation has not been observed for Rh/CeO_2. As such, one might expect that the methanation on Rh/CeO_2 follows a carbon monoxide pathway. However, some activity was also observed from formate. While not excluding the carbon monoxide pathway, it does suggest that several pathways might be involved and perhaps interact with each other, by reactions such as $HCOO \rightleftharpoons CO + OH$.

The Ce^{4+}/Ce^{3+} cycling of CeO_2 could be a contributing factor in the promotion of CeO_2 for both methanation as well as rWGS. As was seen, CO formation at the Rh-CeO_2 interface as well as surface carbonates responded to the hydrogen stimulus. A potential mechanism could be the activation of CO_2 by an oxygen vacancy on the CeO_2 surface which is later on hydrogenated by H_2 spill-over from the Rh metal. A similar mechanism has been proposed for other catalysts[56], in which the oxygen vacancy is formed and healed in the reaction cycle. Similar behaviour was observed in the HE-XRD results, in which CeO_2 was partially re-oxidised during when H_2 was removed from the gas stream.

While leaving gaps for further exploration, the results of this work have provided an insight into the mechanisms behind the reaction pathway of CO_2 methanation over Rh/CeO_2.

5 Conclusions and future work

The structural changes of the Rh/CeO_2 catalyst and its surface reactions during CO_2 methanation were studied *in situ* by HE-XRD, AP-XPS and DRIFTS. It was revealed that CeO_2 takes an active role, cycling between Ce^{4+} and Ce^{3+}. Presumably, this is due to the formation of oxygen vacancies which are further on partially healed by an intermediate involving reaction. Furthermore, while the rhodium was shown to be predominately in a reduced state during the reaction, a RhO_x phase was observed. This RhO_x could not be removed by reduction and is likely located at the intermediary region of Rh and CeO_2, caused by a strong metal support interaction.

The presence of active carbon monoxides on the catalyst strongly suggests that the catalyst follows a carbon monoxide pathway, possibly the carbide pathway. The Ce^{4+} and Ce^{3+} of CeO_2 affected the configuration of adsorbed carbonates, alternating between b-CO_3 and p-CO_3. If these carbonates also take part in the methanation reaction remains unknown. While some activity of formate could be observed, this is possibly due to an equilibrium reaction such as $HCOO \rightleftharpoons CO + OH$ rather than a support for the formate pathway being present. Furthermore, the formation of this formate could have been alleviated by CO_2 activation by the reduced CeO_2, possibly involving a short-lived bicarbonate (HCO_3) intermediate as reported for other catalysts [25].

5.1 Remaining questions

While a greater insight into the mechanisms of CO_2 methanation on Rh/CeO_2 has been gained, the complete reaction pathway remains unknown. Several kinds of surface carbon monoxide species were identified but their interactions, or lack thereof, to each other are not clear. As such, it cannot be stated whether or not only a few participate in a reaction step while the others respond due to processes such as reconfiguration and migration. Furthermore, the active sites remain elusive. The occurrence of CO in the rhodium-ceria interface suggests that CO_2 dissociation may occur in this catalytic site environment. If hydrogenation also occur on these sites or if the CO migrates to another site for hydrogenation is still unknown. A study of a potential migration on a model catalyst would therefore be of interest.

In this work, the MES-DRIFTS was performed using H_2 modulation in order to repeat the previous work in which the structural changes were characterised. While allowing one to find active species, the sequencing of the reaction pathway becomes daunting due to hydrogen being involved in several reaction steps. As

such, one should follow this study with a CO_2 modulated MES study as the linear path of C greatly simplifies the process.

Given that the pathway is determined, the determination of the limiting step(s) would be of interest. For instance, how does ceria promote the hydrogenation on rhodium? Is it primarily an electronic promotion or is it some other process, such as CO_2 dissociation at the Rh-CeO_2 interface, which provides the greatest beneficial effect? This is a highly complex question which is not easily answered by experiments alone.

Acknowledgements

This research was funded by the Knut and Alice Wallenberg foundation through the project "Atomistic design of Catalysts" (No. 2015.0058) and the Swedish Research Council through the Röntgen-Ångström collaboration “Synergistic development of X-ray techniques and applicable thin oxides for sustainable chemistry” (No. 2017-06709).

Competence Centre for Catalysis, which is hosted by Chalmers University of Technology and financially supported by the Swedish Energy Agency and the member companies: AB Volvo, ECAPS AB, Johnson Matthey AB, Preem AB, Scania CV AB, Umicore AG & Co. KG and Volvo Car Corporation AB

Parts of the work have also been performed at the synchrotron research facilities PETRA III (DESY) and ALS. The provision of beamtime as well as assistance from beamline scientists is gratefully acknowledged.

I would also like to thank:

My supervisor Per-Anders Carlsson and examiner Magnus Skoglundh for all their help and guidance in my research. Your input has been invaluable.

Lennart Norberg, Lasse Urholm and Ulf Stenman, without their help in setting up equipment this work would have ground into a halt.

All my current and previous colleagues at TYK and KCK, especially Adam, Alvaro, Andreas, Anne, Carl-Robert, Colin, David, Ida, Johanna, Leo, Mats, Natalia, Peter, Simone and Xueting for all your help and stimulating discussions.

Finally, my family for all their love support all throughout my life.

Felix Hemmingsson, Göteborg, May 2020

Bibliography

(1) Artz, J.; Müller, T. E.; Thenert, K.; Kleinekorte, J.; Meys, R.; Sternberg, A.; Bardow, A.; Leitner, W. *Chemical Reviews* **2018**, *118*, 434–504 (cit. on p. 1).

(2) Wang, W.; Wang, S.; Ma, X.; Gong, J. *Chem. Soc. Rev.* **2011**, *40*, 3703–3727 (cit. on p. 1).

(3) Kannan, N.; Vakeesan, D. *Renewable and Sustainable Energy Reviews* **2016**, *62*, 1092–1105 (cit. on p. 1).

(4) Lund, P. D.; Lindgren, J.; Mikkola, J.; Salpakari, J. *Renewable and Sustainable Energy Reviews* **2015**, *45*, 785–807 (cit. on p. 1).

(5) Orecchini, F. *International Journal of Hydrogen Energy* **2006**, *31*, 1951–1954 (cit. on p. 1).

(6) Abe, J.; Popoola, A.; Ajenifuja, E.; Popoola, O. *International Journal of Hydrogen Energy* **2019**, *44*, 15072–15086 (cit. on p. 1).

(7) Kirubakaran, A.; Jain, S.; Nema, R. *Renewable and Sustainable Energy Reviews* **2009**, *13*, 2430–2440 (cit. on p. 1).

(8) Villante, C.; Genovese, A. *International Journal of Hydrogen Energy* **2012**, *37*, Hydrogen Enriched Methane, 11541–11548 (cit. on p. 1).

(9) Utgikar, V. P.; Thiesen, T. *Technology in Society* **2005**, *27*, 315–320 (cit. on p. 1).

(10) Pasman, H. J.; Rogers, W. J. *Journal of Loss Prevention in the Process Industries* **2010**, *23*, Papers Presented at the 2009 International Symposium of the Mary Kay O'Connor Process Safety Center, 697–704 (cit. on p. 1).

(11) San Marchi, C.; Hecht, E.; Ekoto, I.; Groth, K.; LaFleur, C.; Somerday, B.; Mukundan, R.; Rockward, T.; Keller, J.; James, C. *International Journal of Hydrogen Energy* **2017**, *42*, Special issue on The 6th International Conference on Hydrogen Safety (ICHS 2015), 19-21 October 2015, Yokohama, Japan, 7263–7274 (cit. on p. 1).

(12) Vogt, C.; Monai, M.; Kramer, G. J.; Weckhuysen, B. M. *Nature Catalysis* **2019**, *2*, 188–197 (cit. on pp. 1, 2, 5, 6).

(13) Verhelst, S.; Turner, J. W.; Sileghem, L.; Vancoillie, J. *Progress in Energy and Combustion Science* **2019**, *70*, 43–88 (cit. on pp. 1, 2).

(14) Yaws, C. L. In *Yaws' Critical Property Data for Chemical Engineers and Chemists*; Knovel: 2012 (cit. on p. 1).

(15) Hänggi, S.; Elbert, P.; Bütler, T.; Cabalzar, U.; Teske, S.; Bach, C.; Onder, C. *Energy Reports* **2019**, *5*, 555–569 (cit. on p. 2).

(16) The Sabatier System: Producing Water on the Space Station, NASA.gov NASA, https://www.nasa.gov/mission_pages/station/research/news/sabatier.html (accessed 17/05/2020) (cit. on p. 2).

(17) Blanco, H.; Faaij, A. *Renewable and Sustainable Energy Reviews* **2018**, *81*, 1049–1086 (cit. on p. 2).

(18) Yaws, C. L. In *Yaws' Critical Property Data for Chemical Engineers and Chemists*; Knovel: 2012 (cit. on p. 2).

(19) Chorkendorff, I.; Niemantsverdriet, J., *Concepts of Modern Catalysis and Kinetics*; Wiley: 2017 (cit. on pp. 2, 3, 6, 9, 11).

(20) Seemann, M.; Thunman, H. In *Substitute Natural Gas from Waste*, Materazzi, M., Foscolo, P. U., Eds.; Academic Press: 2019, pp 221–243 (cit. on pp. 3, 5).

(21) Rönsch, S.; Schneider, J.; Matthischke, S.; Schlüter, M.; Götz, M.; Lefebvre, J.; Prabhakaran, P.; Bajohr, S. *Fuel* **2016**, *166*, 276–296 (cit. on pp. 3, 5, 6).

(22) Paul Sabatier – Nobel Lecture, NobelPrize.org Nobel Media AB, https://www.nobelprize.org/prizes/chemistry/1912/sabatier/lecture/ (accessed 17/05/2020) (cit. on p. 5).

(23) Varvoutis, G.; Lykaki, M.; Stefa, S.; Papista, E.; Carabineiro, S. A.; Marnellos, G. E.; Konsolakis, M. *Catalysis Communications* **2020**, *142*, 106036 (cit. on p. 5).

(24) Younas, M.; Loong Kong, L.; Bashir, M. J. K.; Nadeem, H.; Shehzad, A.; Sethupathi, S. *Energy & Fuels* **2016**, *30*, 8815–8831 (cit. on p. 5).

(25) Baraj, E.; Vagaský, S.; Hlinčík, T.; Ciahotný, K.; Tekáč, V. *Chemical Papers* **2016**, *70*, 395–403 (cit. on pp. 5, 6, 27).

(26) Frontera, P.; Macario, A.; Ferraro, M.; Antonucci, P. *Catalysts* **2017**, *7*, 59 (cit. on p. 5).

(27) Barrientos, J.; Lualdi, M.; Suárez París, R.; Montes, V.; Boutonnet, M.; Järås, S. *Applied Catalysis A: General* **2015**, *502*, 276–286 (cit. on p. 5).

(28) Kattel, S.; Yan, B.; Yang, Y.; Chen, J. G.; Liu, P. *Journal of the American Chemical Society* **2016**, *138*, PMID: 27571313, 12440–12450 (cit. on p. 6).

(29) Thomas, J.; Thomas, W., *Principles and Practice of Heterogeneous Catalysis*; Wiley: 2014, p 41 (cit. on p. 7).

(30) Ertl, G.; Knözinger, H.; Weitkamp, J., *Preparation of Solid Catalysts*; Wiley: 2008 (cit. on p. 9).

(31) Wakihara, T.; Ihara, A.; Inagaki, S.; Tatami, J.; Sato, K.; Komeya, K.; Meguro, T.; Kubota, Y.; Nakahira, A. *Crystal Growth & Design* **2011**, *11*, 5153–5158 (cit. on p. 9).

(32) Marceau, E.; Carrier, X.; Che, M. In *Synthesis of Solid Catalysts*; John Wiley & Sons, Ltd: 2009; Chapter 4, pp 59–82 (cit. on p. 9).

(33) Landau, M. V. In *Synthesis of Solid Catalysts*; John Wiley & Sons, Ltd: 2009; Chapter 5, pp 83–109 (cit. on p. 9).

(34) Hermans, S. In *Synthesis of Solid Catalysts*; John Wiley & Sons, Ltd: 2009; Chapter 8, pp 153–171 (cit. on p. 9).

(35) Smart, L.; Moore, E., *Solid State Chemistry: An Introduction, Fourth Edition*; CRC Press: 2016 (cit. on p. 10).

(36) Bragg, W. H.; Bragg, W. L. *Proceedings of the Royal Society of London. Series A, Containing Papers of a Mathematical and Physical Character* **1913**, *88*, 428–438 (cit. on p. 10).

(37) Encyclopædia Britannica, 2018 (cit. on p. 11).

(38) Karslıoğlu, O.; Bluhm, H. In *Operando Research in Heterogeneous Catalysis*, Frenken, J., Groot, I., Eds.; Springer International Publishing: Cham, 2017, pp 31–57 (cit. on p. 11).

(39) Watts, J.; Wolstenholme, J., *An Introduction to Surface Analysis by XPS and AES*; Wiley: 2019 (cit. on p. 11).

(40) Wachsman, E., *Solid State Ionic Devices 6 – Nano Ionics*; ECS transactions; Electrochemical Society: 2009, p 256 (cit. on p. 11).

(41) Larkin, P. J. In *Infrared and Raman Spectroscopy (Second Edition)*, Larkin, P. J., Ed., Second Edition; Elsevier: 2018, pp 7–28 (cit. on pp. 11, 13).

(42) Höpe, A. In *Spectrophotometry*, Germer, T. A., Zwinkels, J. C., Tsai, B. K., Eds.; Experimental Methods in the Physical Sciences, Vol. 46; Academic Press: 2014, pp 179–219 (cit. on pp. 11, 12).

(43) Larkin, P. J. In *Infrared and Raman Spectroscopy (Second Edition)*, Larkin, P. J., Ed., Second Edition; Elsevier: 2018, pp 75–84 (cit. on p. 13).

(44) Müller, P.; Hermans, I. *Industrial & Engineering Chemistry Research* **2017**, *56*, 1123–1136 (cit. on p. 14).

(45) Baurecht, D.; Porth, I.; Fringeli, U. *Vibrational Spectroscopy* **2002**, *30*, Papers Presented at the 1st International Conference on Advanced Vibrational Spectroscopy, Turku, Finland, August 19-24, 2001, 85–92 (cit. on pp. 14, 15).

(46) Baurecht, D.; Fringeli, U. P. *Review of Scientific Instruments* **2001**, *72*, 3782–3792 (cit. on p. 15).

(47) Urakawa, A.; Bürgi, T.; Baiker, A. *Chemical Engineering Science* **2008**, *63*, 5TH Unsteady-State Processes in Catalysis: a Special Issue of Chemical Engineering Science, 4902–4909 (cit. on p. 15).

(48) Martin, N. M.; Velin, P.; Skoglundh, M.; Bauer, M.; Carlsson, P.-A. *Catal. Sci. Technol.* **2017**, *7*, 1086–1094 (cit. on p. 17).

(49) Kiennemann, A.; Breault, R.; Hindermann, J.-P.; Laurin, M. *J. Chem. Soc., Faraday Trans. 1* **1987**, *83*, 2119–2128 (cit. on pp. 19, 23).

(50) Krenn, G.; Bako, I.; Schennach, R. *The Journal of Chemical Physics* **2006**, *124*, 144703 (cit. on pp. 21, 23).

(51) Beutler, A.; Lundgren, E.; Nyholm, R.; Andersen, J.; Setlik, B.; Heskett, D. *Surface Science* **1998**, *396*, 117–136 (cit. on p. 21).

(52) Fisher, I. A.; Bell, A. T. *Journal of Catalysis* **1996**, *162*, 54–65 (cit. on p. 23).

(53) Binet, C.; Daturi, M.; Lavalley, J.-C. *Catalysis Today* **1999**, *50*, 207–225 (cit. on p. 23).

(54) Li, C.; Sakata, Y.; Arai, T.; Domen, K.; Maruya, K.-i.; Onishi, T. *J. Chem. Soc., Faraday Trans. 1* **1989**, *85*, 929–943 (cit. on p. 23).

(55) Araiza, D. G.; Gómez-Cortés, A.; Díaz, G. *Catal. Sci. Technol.* **2017**, *7*, 5224–5235 (cit. on p. 23).

(56) Ye, J.; Liu, C.; Mei, D.; Ge, Q. *ACS Catalysis* **2013**, *3*, 1296–1306 (cit. on p. 25).

Notation

δ(X)	Symmetric in-plane bending, scissoring, of group X
ν_s(X)	Symmetric stretching of group X
ν_{as}(X)	Asymmetric stretching of group X
ϕ_k^{PSD}	The operator controlled phase angle/phase angle for demodulation for the k^{th} harmonic frequency
$\tilde{\nu}$	Wavenumber, reciprocal wavelength
φ_k	Phase delay in regards to the k^{th} harmonic frequency
$A_k^{\phi_k^{PSD}}$	The phase-resolved amplitudal data for a given operator controlled angle and harmonic frequency
d	Interplanar distance in a crystal structure
y_i	Partial gas composition in regards to substance i. Expressed as molar or volumetric percent of the gas that is constituted by i
DRIFTS	Diffuse reflectance infrared Fourier transform spectroscopy
MES	Modulation excitaion spectroscopy
PSD	Phase sensitive detection